Journal of Alloys and Compounds 911 (2022) 164950

Contents lists available at ScienceDirect

Journal of Alloys and Compounds

journal homepage: www.elsevier.com/locate/jalcom

Vanadium trapped by oblique nano-sheets to preserve the anisotropy in Co–V thin films at high temperature

C. Favieres[a,b,*], J. Vergara[a,b], C. Magén[c,d,e], M.R. Ibarra[c,d,e], V. Madurga[a]

[a] Laboratory of Magnetism, Department of Science (Physics), Public University of Navarre (UPNA), Campus de Arrosadía, E-31006 Pamplona, Spain
[b] Institute for Advanced Materials and Mathematics (INAMAT2), Public University of Navarre (UPNA), Campus de Arrosadía, E-31006 Pamplona, Spain
[c] Instituto de Nanociencia y de Materiales de Aragón (INMA) CSIC-Universidad de Zaragoza, 50009 Zaragoza, Spain
[d] Departamento de Física de la Materia Condensada, Universidad de Zaragoza, 50009 Zaragoza, Spain
[e] Laboratorio de Microscopías Avanzadas (LMA), Universidad de Zaragoza, 50018 Zaragoza, Spain

ARTICLE INFO

Article history:
Received 30 December 2021
Received in revised form 12 March 2022
Accepted 7 April 2022
Available online 12 April 2022

Keywords:
Thin films
Nano-fabrications
Anisotropy
Electrical transport
Scanning tunnelling microscopy, STM
Transmission electron microscopy, TEM
Electron energy loss spectroscopy, EELS

ABSTRACT

In this study, oriented nano-sheets generated during the growth of cobalt-rich Co–V and Co–Zn thin films induced a large anisotropy in the magnetic and transport properties. The regular nano-sheets were tilted 52–54 deg. with respect to the substrate plane, ≈ 3.0–4.0 nm thick, ≈ 30–100 nm wide, and ≈ 200–300 nm long, with an inter-sheet distance of ≈ 0.9–1.2 nm. In spite of the different microstructures of the two kinds of samples where the Co–V films were amorphous, whereas the Co–Zn films showed a growth of Zn nanocrystals, the oblique nano-sheet morphology conferred noticeable shape anisotropy to both specimens. This anisotropy resulted in an in-plane uniaxial magnetic anisotropy. The changes in the nano-morphology caused by thermal treatments, and hence in their anisotropic properties, were studied. While the Co–V samples retained or increased their magnetic and transport anisotropies, this anisotropic behavior vanished for the annealed Co–Zn films. High resolution transmission electron microscopy, HRTEM, including chemical analysis at the nano-scale, and the dependence of the anisotropic resistance on temperature allowed to establish the nature and the activation energy spectra of the atomic relaxation processes during heating. These processes displayed a single peak at 1.63 eV for the Co–V and two peaks at 1.67 and 2.0 eV for the Co–Zn. These spectra and their singularities were associated to the changes induced in the nano-morphology of the films by thermal treatments. The Co–V films retained their nano-sheet morphology almost up to 500 ºC; the Co–Zn films lost their nano-sheets at 290 ºC. The thermal stability exhibited by the Co–V films makes them useful for applications in ultra high frequency, optical, magnetostrictive and magneto-electric devices.

1. Introduction

The improvement of materials with tailored physical properties at the nanoscale represents a key field in science and technology. In particular, magnetic materials in the form of nanoparticles, nanodots, nanowires, thin films, multilayers, etc. are continuously being developed due to their versatile applications in data storage technology, magnetic field sensing, high-frequency devices, and spintronics, among many others [1–7]. Furthermore, controlling the magnetization direction of materials with nano-sized constituents is an interesting objective from both a theoretical and applied point of view; the latter is interesting because the magnetization direction significantly influences the performance of multiple magnetic devices [8–15]. Intermetallic magnetic alloys and compounds such as Co–V and Co–Zn, have been demonstrated to exhibit magnetic properties which are known to be highly dependent on their special size and shape, i.e., bulk or nanoparticulated [16], thin films [17,18], and nanowires [19,20]. In this regard, much attention has been paid to the impact of the synthesis techniques on the morphology of the materials. In particular, oblique-angle incidence techniques have been demonstrated to be very suitable for the growth of films exhibiting special physical properties associated with their morphology and micro- or nanostructure [21–29].

The oblique Pulsed Laser Deposition (PLD) technique has allowed us to fabricate ferromagnetic thin films formed by oriented nano-

* Corresponding author at: Laboratory of Magnetism, Department of Science (Physics), Public University of Navarre (UPNA), Campus de Arrosadía, E-31006 Pamplona, Spain.
E-mail addresses: favieresc@unavarra.es (C. Favieres), jvergara@unavarra.es (J. Vergara), cmagend@unizar.es (C. Magén), ibarra@unizar.es (M.R. Ibarra), vmadurga@unavarra.es (V. Madurga).

https://doi.org/10.1016/j.jallcom.2022.164950
0925-8388/

sheets [24,30–33]. By means of Scanning Tunneling Microscopy (STM) and High Resolution Transmission Electron Microscopy (HRTEM), we discovered that Co obliquely deposited films were formed by nano-sheets, with dimensions of ≈ 300 × 80 × 5 nm for each nano-sheet, separated by free-space regions approximately 1.5 nm wide and oriented ≈ 60 deg. with respect to the substrate plane [31,32]. This nano-morphology was generated thanks to our particular geometry during deposition and the arrangement of the laser beam, the target, and the laboratory-designed substrate-holder [31]. Indeed, the particular position of the substrates on the lateral surface of the cone with its axis of rotational symmetry parallel to the plasma flux direction caused the growth direction of our oblique nano-sheets (always occurring towards the plasma source) to retain a constant angle with respect to the direction of growth of the nano-sheets observed in previous stages. The Cylindrical Symmetry Oblique Growth films with these nano-sheets will be referred to as CSOG films throughout this work. Co and Co-rich CSOG films showed in-plane uniaxial magnetic anisotropy (UMA) and mechanical, transport, and optical anisotropies whose origin lay in the morphology of oblique nano-sheets. In effect, these as-deposited Co CSOG films, which were amorphous, exhibited in-plane UMA fields up to $H \approx 80$ kAm^{-1} and notable anisotropy in their resistivity: In the as-deposited state, they had a large resistivity (≈130 μOhm·cm) when the electric current flowed along the perpendicular direction of the nano-sheets, while the resistivity parallel to the nano-sheets was approximately 30% smaller [32]. Additionally, by STM, we observed that CSOG Co films' surfaces looked like nano-strings (≈300 nm long, 12 nm width) [24,31,32]. Our studies allowed us to confirm that their anisotropic physical properties had their origin in the internal nano-morphology, and not exclusively linked to a surface nano-morphology. Furthermore, we showed that the nano-sheet morphology and the anisotropic properties disappeared after annealing the Co samples at ≈ 270 ºC [32].

In a previous work [31], we also found that as-deposited Co–V and Co–Zn CSOG films exhibited well-defined in-plane UMA. However, both kinds of samples behaved completely differently after being subjected to annealing: Interestingly, the Co–V films substantially increased their UMA after annealing at temperatures of 350, 400, and 450 °C, and in contrast, the Co–Zn films lost their UMA after being heated at 290–300 ºC.

In the present work, we report that, besides this magnetic anisotropy, these Co–V and Co–Zn CSOG samples also exhibited anisotropic transport behaviors. We shall demonstrate that the origin of these anisotropies lies in the films' special nano-morphology comprised of oriented nano-sheets, although the inner structure of the films is different for the Co–V and Co–Zn films. Furthermore, the changes of this nano-morphology with thermal treatments and consequently, the changes in these anisotropic properties, are visualized and analyzed, presenting the activation energy spectra of the atomic processes during heating.

The structural relaxation processes that are produced in Co–V and Co–Zn CSOG thin films when their temperature increases, which irreversibly change some magnitudes, for example, their electrical resistance, are assumed in this work to be the irreversible processes of atom diffusion. These atomic displacements occur from their metastable energetically high positions (due to the amorphous or nano-crystalline structure of the as-deposited films, which are out of thermodynamic equilibrium) to other positions with lower energy, including the amorphous or nano-crystalline relaxed structures, or, finally, to the energetically lowest atom positions corresponding to the thermodynamically stable crystalline and alloyed films.

We shall show and discuss the significant differences that the thermal treatments produce in terms of the nano-sheet morphology and the structure of both kinds of samples and we shall show that, whereas in the Co–V CSOG films, the magnetic and electrical anisotropies are retained and even increased, in the Co–Zn CSOG films, these anisotropic properties are lost. The thermal stability exhibited by the Co–V films makes them useful for applications in ultra high frequency, optical, magnetostrictive and magneto-electric devices.

2. Experimental procedures

Thin films of Co-rich, Co–MT (MT = V or Zn) were grown in a PLD chamber by oblique angle incidence, in particular CSOG films. A detailed description of the experimental conditions employed for the fabrication of the samples can be found in Ref. [31], especially those concerning the relative arrangement and spatial symmetries of the laser beam, target, and substrates, which allowed us to control the generation of these CSOG films. A *Quantel Brilliant* pulsed Nd–YAG laser (λ = 1064 nm, 20 Hz repetition rate, 5 ns pulse and an energy of 220 mJ/pulse in the target's spot, ≈12 mm^2 area, laser fluence ≈1.8 J·cm^{-2}) and a *Neocera* stainless-steel chamber at a base pressure of 10^{-6} mbar were used. Two foils constituted the rotating target of 32 rpm, one above the other. Both foils (*Goodfellow Ltd.*) were mechanically polished before the ablation processes. The bottom foil was the corresponding metal MT (99.8% pure V or 99.95% pure Zn), and the top foil was a Co one (99.99% pure) in which circular holes, all with the same diameter, were made and uniformly distributed on the Co foil surface. The area corresponding to the MT, which was that corresponding to the holes, was 14% of the total target's area. During PLD, the laser's spot always reached both foils of Co and MT simultaneously, with an angle of 45 deg. Therefore, after the laser impact, a mixture of Co and MT was ejected toward the substrates at the same time. The thin films were simultaneously deposited (in most cases) for 20 min over glass and Si substrates placed in the substrate-holder. The glass substrates were 7 mm in diameter and 0.13 mm thick. The single crystalline Si (111) substrates were 20 × 8 × 0.5 mm^3. All of them were placed at a distance of 70 mm from the target. Films at 0 deg. (perpendicular-deposited) and CSOG films at 55 deg. (oblique-deposited) with respect to the normal to the substrate were produced simultaneously. The films deposited on glass were used for magnetic and electric characterization, as well as for HRTEM and STM. The films deposited on Si substrates were used for X-ray diffraction studies (XRD). The thickness of a pure Co sample—60 nm—was measured using an atomic force microscope and from the HRTEM results.

All of the samples were characterized structurally, magnetically, and electrically in the as-deposited state and after being heated in a dynamic Ar atmosphere at temperatures of 400, 450 and 500 °C at a heating rate of 10 ºC·min^{-1}. Once this temperature was reached, the films were removed from the hot region of the furnace and kept in the Ar atmosphere until they were slowly cooled.

The structure of the samples was investigated by means of XRD (*XRD-3003 Seifert diffractometer*) in the grazing incidence mode (angle 1.0 deg.) with Cu Kα radiation operating at 40 kV and 35 mA, with a scan step of 0.1 deg. A graphite secondary mono-chromator was placed before the detector. STM was performed by means of a Metris 100 (*Burleigh Fishers, NY, USA*) microscope to examine the surface morphology of the films deposited on glass substrates.

HRTEM experiments were performed in an image-corrected Thermo Fisher Titan Cubed 60–300, operated at 300 kV. Cross-sectional specimens were prepared for HRTEM observations by mechanical polishing and Ar^+ ion milling. Electron Energy Loss Spectroscopy, EELS, at nanoscale was also performed from the cross sectional prepared samples.

The CSOG films were magnetically characterized by measuring the *M-H* hysteresis loops at room temperature with an *EG&G* Vibrating Sample Magnetometer (VSM). The magnetic field was applied parallel to the plane of the films. By rotating the film around the normal to its plane inside the magnetic field, it was possible to find the in-plane easy and hard directions of magnetization. The

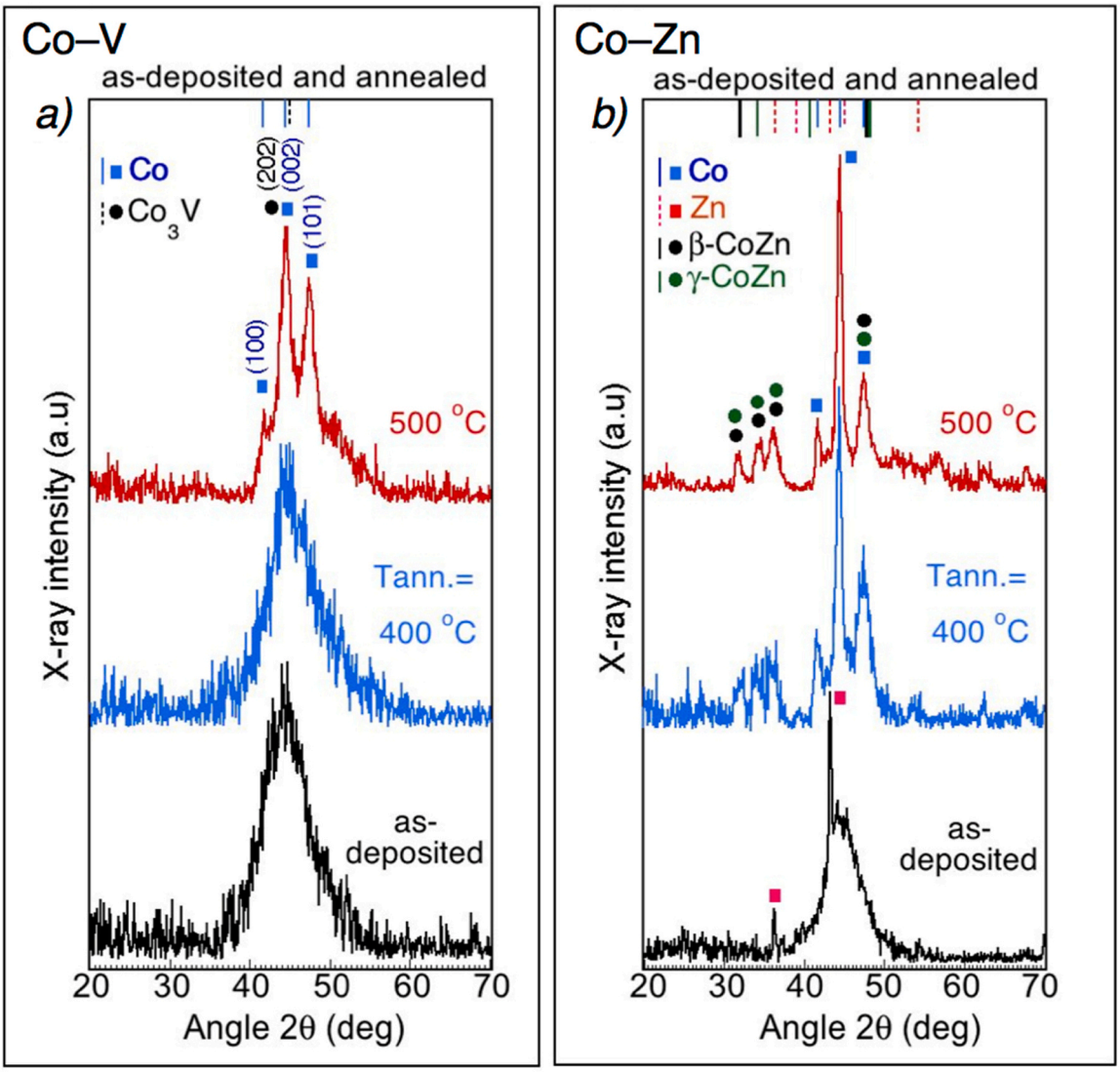

Fig. 1. X-ray diffraction (XRD) measurements corresponding to the as-deposited and annealed (T_{ann} = 400 ºC and 500 ºC) CSOG films of (a) Co–V and (b) Co–Zn. The solid and dashed lines marked on the upper side of the graphics indicate the angles of the XRD peaks for pure Co, Zn, CoV, and CoZn phases, respectively. The peaks corresponding to the Co (100), Co (002), Co (101), Co_3V (202), β-CoZn, and γ-CoZn phases are marked.

magnetic anisotropy field, $H_{k,}$ was determined from the H value in the crossover in the M vs H hard loop.

The saturation magnetization of a perpendicular-deposited, θ = 0 deg, Co film was $\mu_0 M_{s,Co,per} \approx 1.4$ T [31]; for Co CSOG film, $\mu_0 M_{s,Co,CSOG} \approx 0.8$ T; after annealing at 450 ºC, $\mu_0 M_{s,Co,per,ann.} \approx 1.7$ T and $\mu_0 M_{s,Co,CSOG,ann.} \approx 1.7$ T. For the Co–V films, $\mu_0 M_{s,Co-V,per} \approx 1.0$ T, $\mu_0 M_{s,Co-V,CSOG} \approx 0.6$ T, and after annealing, $\mu_0 M_{s,Co-V,per,ann.} \approx 1.2$ T and $\mu_0 M_{s,Co-V,CSOG,ann.} \approx 0.9$ T. For Co–Zn films, $\mu_0 M_{s,Co-Zn,per} \approx 0.8$ T and $\mu_0 M_{s,Co-Zn,CSOG} \approx 0.6$ T and after annealing $\mu_0 M_{s,Co-Zn,per,ann.} \approx 1.1$ T and $\mu_0 M_{s,Co-Zn,CSOG,ann.} \approx 1.1$ T. According to the AFM and HRTEM results, we used ≈ 50 nm for the thickness of these perpendicular-deposited films and ≈ 24 nm for these oblique-deposited films. The uncertainty of the previous $\mu_0 M_s$ values was not lower than ± 0.1 T for all of the cases due to the use of the measured thickness of the deposited film, the area of the substrate's surface, and the magnetic moment of each sample.

Transport characterization of the CSOG films was carried out by measuring their electrical resistance R. R of the films deposited over the glass substrates was measured, at room temperature, between two contacts separated by 4.5 mm. R took different values, depending on the direction in which it was measured: Parallel to the nano-sheet direction, $R_{||}$, or perpendicular to the nano-sheets, $R_{\perp}$. The values of $R_{||}$ and $R_{\perp}$ were also measured at room temperature after annealing the samples at 450 °C. The four-probe technique provided the same results for all of the cases.

The dependence of R of the samples on temperature was also measured by placing the samples in a furnace. To avoid oxidation phenomena, the films were kept in a dynamic inert Ar atmosphere during the whole annealing process and until they were removed from the furnace. The heating rate was 10 ºC·min^{-1}.

3. Results and discussion

3.1. Microstructure and nano-morphology

Fig. 1 shows the XRD patterns of the Co–V and Co–Zn CSOG films. They were analyzed in the as-deposited state and after being annealed at different temperatures up 500 °C.

Fig. 1(a) shows that the as-deposited Co–V CSOG film (black curve) exhibited a halo centered at 2θ ≈ 45 deg., mainly corresponding to amorphous Co and to Co–V [31]. No peaks corresponding to Co, V, or CoV phases were detected. It is also seen that after annealing these films at 400 °C, (blue curve in Fig. 1(a)), they were still amorphous in nature. In contrast, after annealing the Co–V

films at 500 °C (red curve in Fig. 1(a)) three peaks appeared. They corresponded to Co and Co_3V *hcp* crystals. The most intense one (at 2θ = 44.4 deg.) corresponded to a mixture of Co (002) and probably to the intermetallic Co_3V *hcp* phase, with the peak corresponding to the (202) planes [16,31,34,35]. Applying the Scherrer's formula [36] to the Co (002) and Co_3V (202) peaks, the crystal size of $t \approx 4.6$ nm was estimated. A similar value ($t \approx 4.3$ nm) was obtained from the Co (101) peak.

The as-deposited Co–Zn CSOG film displayed evidence of *hcp* Zn crystallites in the amorphous matrix (see Fig. 1(b), black bottom curve). A peak at 2θ = 43.2 deg., corresponding to Zn (101) planes, and another, less intense peak at 2θ =36.3 deg., which corresponds to Zn (002), were detected. Fig. 1(b) also shows the XRD results of the Co–Zn CSOG film annealed at 400 °C and 500 °C. The disappearance of the pure Zn (101) peak which was present in the as-deposited film was first produced. Second, the growth of *hcp* Co crystals was observed through the most intense peak corresponding to the (002) planes. Third, the growth of β-CoZn and γ-CoZn cubic phases was detected, with the most visible peaks being located between 2θ ≈ 31 and 36 deg. Furthermore, some traces of these crystals could be present, along with Co, in the peak centered at 2θ ≈ 47 deg. [37,38]. The calculated size of the Co crystals corresponding to the (002) and (101) peaks was ≈ 9.8 and ≈ 8.7 nm, respectively.

The HRTEM studies revealed the inner structure and morphology of the films. Results are shown in Fig. 2 for both the Co–V and Co–Zn CSOG samples.

Fig. 2(a) shows that the as-deposited Co–V CSOG films constituted a group of oblique nano-sheets ≈ 3.0 nm thick and ≈ 40 nm wide, with an inter-sheet distance of ≈ 1.1 nm. These nano-sheets were oriented perpendicular to the plane of incidence of the plasma at an angle of ≈ 53 deg. with respect to the substrate plane. This tilted nano-morphology was similar to that discovered in our pure Co CSOG films [31].

The as-deposited Co–Zn CSOG films, Fig. 2(b), were formed by a similar nano-sheet structure. This explains the clear and strong anisotropic magnetic and transport properties of the films ([31] and the present work). Each nano-sheet was ≈ 4.5 nm thick, with an inter nano-sheet distance of ≈ 1.3 nm.

Fig. 3 shows the nano-sheet morphology of the Co–V and Co–Zn CSOG films. Fig. 3(a) and (d) show the STM images of the surfaces of the as-deposited films. The top view of the nano-sheets showed uniform, straight, and long nano-strings as components of the surfaces of the films. Fig. 3(b) and (e) are images of the cross-sections of these films showing a section of each nano-sheet. Combining the images of the nano-strings at the surfaces of the films with the cross-section of the nano-sheets permitted the construction of 3D schematic diagrams of the nano-sheet morphology of the Co–V and Co–Zn CSOG films, see Fig. 3(c) and (f) respectively. Notably, the nano-sheet morphology was the origin of physical anisotropy present in these Co–V and Co–Zn CSOG films, as it was in the case for CSOG Co film [31].

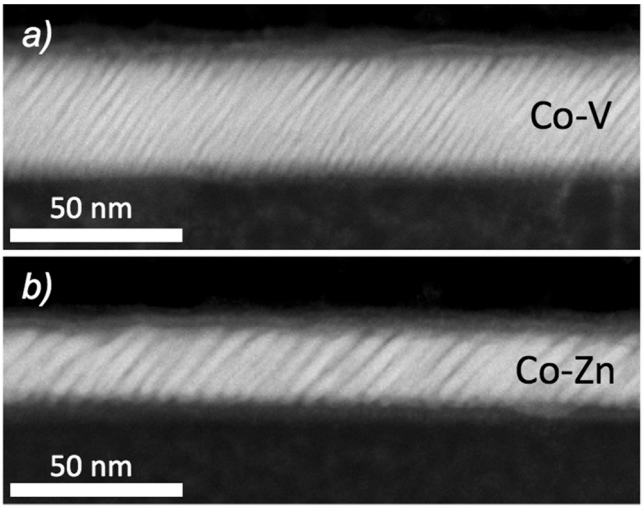

Fig. 2. STEM HAADF cross sectional images of (a) Co–V, and (b) Co–Zn CSOG thin films in the as-deposited state. In both cases, the cross-section of the nano-sheets formed during growth of the films can be seen. Note the relatively high homogeneity of both films for a region of at least 200 nm long.

Fig. 4 shows STEM EELS images of the cross-sections of as-deposited Co–V and Co–Zn CSOG films. The presence and location of their chemical components, cobalt, vanadium, or zinc are shown. Both samples exhibited nano-sheets as constituent, each nano-sheet, notably, possessing a core that was essentially Co-rich. It is worth to note that the nano-sheets were the principal source of anisotropy specially the magnetic anisotropy. This special behavior of Co during the growth of the films (Co coming from a plasma mixture of Co and V or Co and Zn) when forming Co-rich nano-sheets is important with respect to the special anisotropic characteristics it confers on the films (specially magnetic anisotropic characteristics). The Co–V film showed a high concentration of V at the surface of the film, see Fig. 4(a). Moreover, the relative proportion of Co (≈70–80% at.) and V (≈20–30% at.) in the core of the nano-sheets (≈3–4 nm thick), and the high proportion of V present in the inter-nano-sheet space of ≈ 1.2 nm with approximately Co 60% at.–V 40% at., can be clearly seen. In contrast, the Zn content of the Co–Zn CSOG films is much lower. Nano-sheets ≈ 4–5 nm thick, with a Zn relative content of < 2.5% at., separated by an inter-sheet distance of ≈ 2 nm with a relative composition of Co ≈ 93% at.–Zn ≈ 7% at., see Fig. 4(c-d). Accumulation of Zn (some parts crystalline) was found beneath the nano-sheets, at the interface with the substrate 3–5 nm in height. This Zn concentration could be the origin of the Zn crystalline peak present in the X ray diffractogram of the Co–Zn CSOG films—in the as-deposited state—shown in Fig. 1. This particular distribution of Co and Zn in the Co–Zn CSOG film could be considered similar to that corresponding to a CSOG film of pure-Co over a base layer of Zn. The physical behavior of such a Co film over a layer of Zn could be expected to be similar to that shown in Ref. 32 corresponding to the physical behavior of a pure-Co CSOG film. These differences between the structures of Co–V and Co–Zn CSOG films could be the origin of the different behaviors of these two films when heated.

Fig. 5 shows the HRTEM images of Co–V and Co–Zn CSOG films annealed at 450 ºC. The Co–V film retained its nano-sheet morphology, and the isolated nano-sheets began to crystallize. The absence of coalescence of the nano-sheets, in contrast with the behavior of Co CSOG film [32], must have its origin in the addition of V. In the Co–Zn samples, however, the nano-sheet morphology present in the as-deposited films was completely lost after annealing the films. The processes that occurred during annealing the Co–Zn films differed from those found in the Co–V films. For Co–Zn films, similar to what we observed and reported in Ref. 32 for Co CSOG films, the heat treatments provoked a coalescence-like process, with the Co-rich nano-sheets (and a very small amount of Zn in the inter-nano-sheet regions) approaching each other and finally disappearing. This loss of nano-sheets caused a loss of the anisotropy in the magnetic and transport behaviors of the Co–Zn films (as it produced a loss of the anisotropic character of the Co films [32]). The Zn present in the heated film took part in the formation of the β–CoZn, and γ–CoZn crystalline phases, as shown in Fig. 1(b) and 5(b), all of them randomly distributed in the film.

3.2. Anisotropic magnetic behavior

Fig. 6 shows the room-temperature VSM hysteresis loops corresponding to the Co–V and Co–Zn CSOG films, measured in the as-deposited state and after being annealed at 500 °C. In-plane UMA

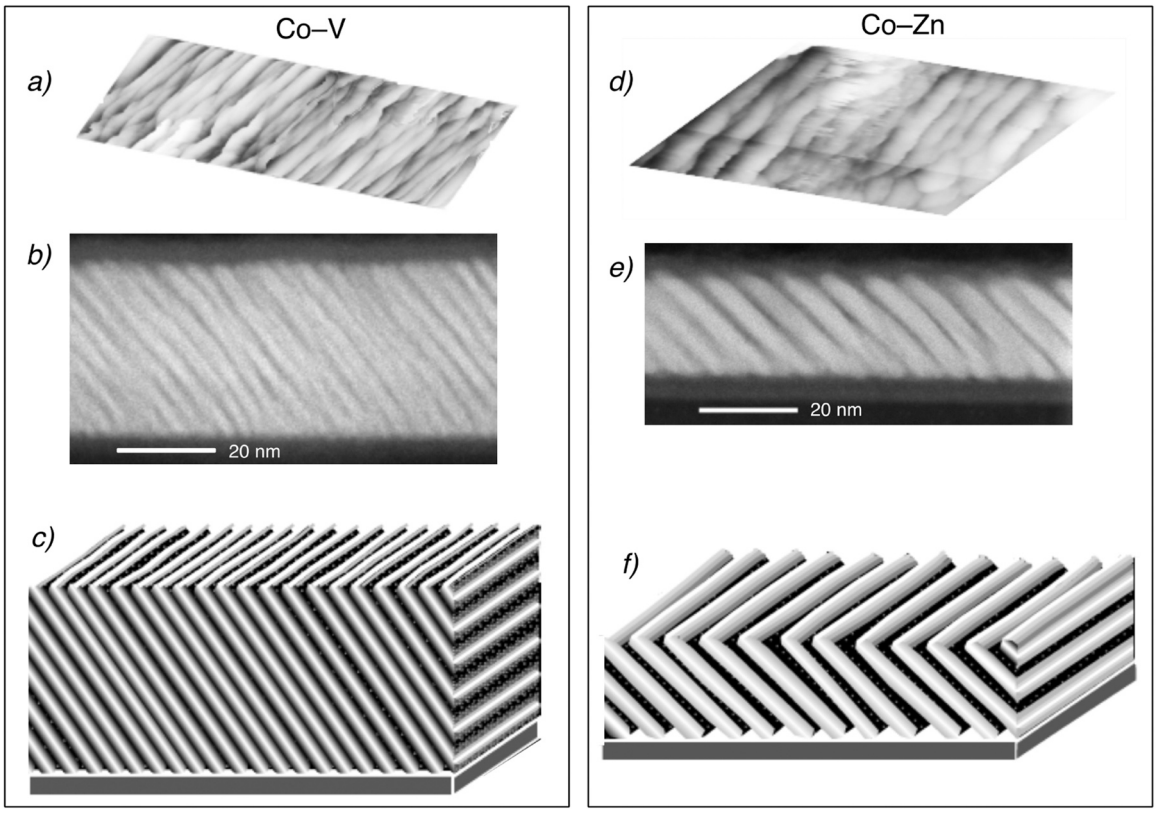

Fig. 3. (a) STM image of the surface of a Co–V CSOG film and (d) an STM image of the surface of a Co–Zn CSOG film. The surfaces formed from nano-strings-like structures can be seen in both images. (b) and (e) Cross-sections of both samples, showing the corresponding internal cross sections of the nano-sheets formed during the growth of the films—STEM HAADF was used to obtain both images. The STM results plus the cross-section results were used to draw two 3D schematic diagrams of the nano-sheet morphology, (c) for Co–V films and (f) for Co–Zn films.

was present in both the as-deposited Co–V films ($\mu_0 H_{k(as\ dep.)} \approx 90{\cdot}10^{-3}$ T) and the as-deposited Co–Zn samples ($\mu_0 H_{k(as\ dep.)} \approx 87{\cdot}10^{-3}$ T) [31]. Although this UMA increased after annealing the Co–V samples to $T_{ann.} = 500\,°C$ ($\mu_0 H_{k\ ann.} \approx 180{\cdot}10^{-3}$ T), it was no longer present in the Co–Zn films.

The origin of this UMA was the shape anisotropy that aligns the magnetization by a magnetostatic effect in the direction of the nano-sheet and in the plane of the film [31 and Figs. 3, 4 and 5 of this work]. The nano-sheets, as the origin of the magnetic anisotropy of our Co and numerous Co-rich films and compounds of Co–metal, were the common morphology amongst them. The two different consequences of the thermal treatments for these samples, preserving the UMA for some of them or eliminating this UMA for others [31], were confirmed and elucidated. One of the most important findings of this work was that this UMA simultaneously increased in the Co–V CSOG films with the permanence and crystallization of Co nano-sheet morphology, whereas the UMA was simultaneously lost with the loss of the nano-sheet morphology for the Co–Zn CSOG samples, see Fig. 5.

In addition to the important behavior of these films regarding their magnetic anisotropic properties, other magnetic features were observed. As shown in Fig. 6(a), the coercive field of the Co–V CSOG films was small in the as-deposited state, $\mu_0 H_{c-\ easy} \approx 1.0{\cdot}10^{-3}$ T, which corresponds to an amorphous-like sample. It increased to $\approx 2.9{\cdot}10^{-3}$ T after being annealed (Fig. 6(b)); this could be attributed to the growth in the Co and Co_3V nano-crystals, see Fig. 1(a) and Fig. 5(a). Additionally, in the as-deposited state, $H_{c\text{-}easy}$ was higher for the Co–Zn ($\mu_0 H_{c-\ easy} \approx 6.0{\cdot}10^{-3}$ T) than for the Co–V, as shown in Fig. 6(a and c). This was probably due to the presence of the non-magnetic Zn nano-crystals which acted to hinder the magnetic domains' wall movements. When the magnetic walls contain such non-magnetic nano-inclusions, the wall energy is reduced because it decreases the area [39, pg. 305]; thus, the wall tends to remain fixed, with higher magnetic fields being necessary to move the walls (higher than in the case of the amorphous Co–V). After the heat treatment, in addition to the important loss of the UMA, an increase in $H_{c\text{-}easy}$ was measured for the Co–Zn CSOG film (Fig. 6(c and d)); in this case, $H_{c\text{-}easy}$ was higher for the Co–V films than for the Co–Zn. This is also related to the grain size; as pointed out above, the *hcp* Co and Co_3V crystals were ≈ 4.6 nm in size. The average size of the Co crystals in the Co–Zn films was ≈ 9.2 nm. It is known that a smaller grain size generates a larger number of grain boundaries and these boundaries impede the domain wall displacements, thus increasing the coercive field [40].

Lastly, an increase in the magnetic moment of these films is visible in Fig. 6(b and d), which had its origin in the growth in the crystallites Co and Co_3V, and Co and β-CoZn γ-CoZn, promoted by the thermal treatment, as a higher degree of crystallinity produced to a higher value for the exchange interaction [41].

3.3. Anisotropic transport properties

3.3.1. Room temperature resistance

Table 1 shows the values of $R_{||}$ and $R_{\perp}$ of the as-deposited and annealed CSOG samples of Co–V and Co–Zn.

Co–V CSOG films, *R (T = 20 ºC)*: For the as-deposited samples, we observed that the Co–V sample exhibited a notable difference between $R_{||}$ and $R_{\perp}$. $(\Delta R/R_{||})_{as\text{-}dep.} = ([R_{\perp} - R_{||}]/R_{||})_{as\text{-}dep.} \approx 33\%$. This anisotropic property, which was also observed in our pure Co CSOG films [32], was caused by the oriented nano-sheet morphology of the films; the electrical conduction increased when the charges moved along a nano-sheet (measuring $R_{||}$) with respect to the situation in

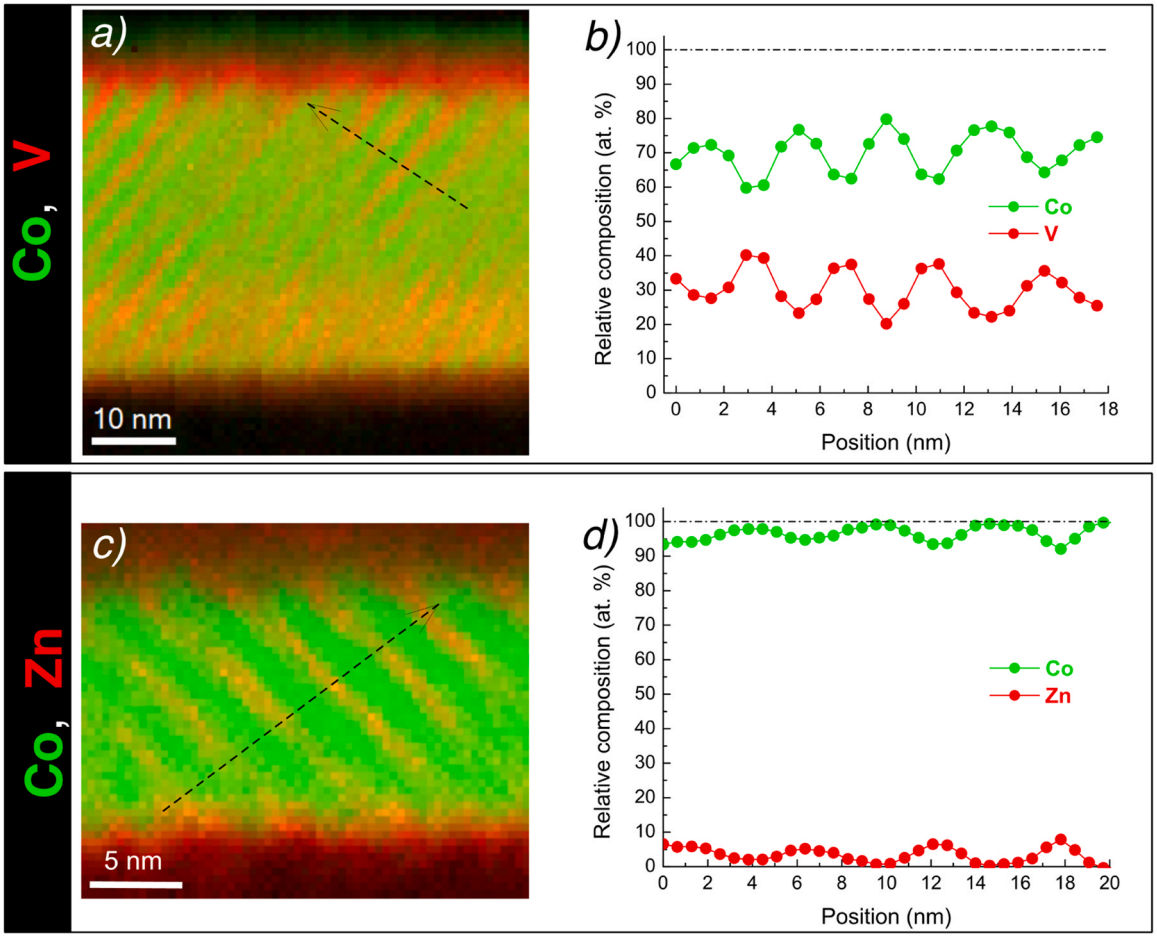

Fig. 4. STEM EELS chemical maps of the cross-sections of the as-deposited CSOG films of (a) Co–V and (c) Co–Zn showing the spatial distribution of their chemical components: cobalt and vanadium and cobalt and zinc, respectively. (b) Co–V and (d) Co–Zn chemical profiles of nano-sheet sections following the dashed arrows in their respective maps.

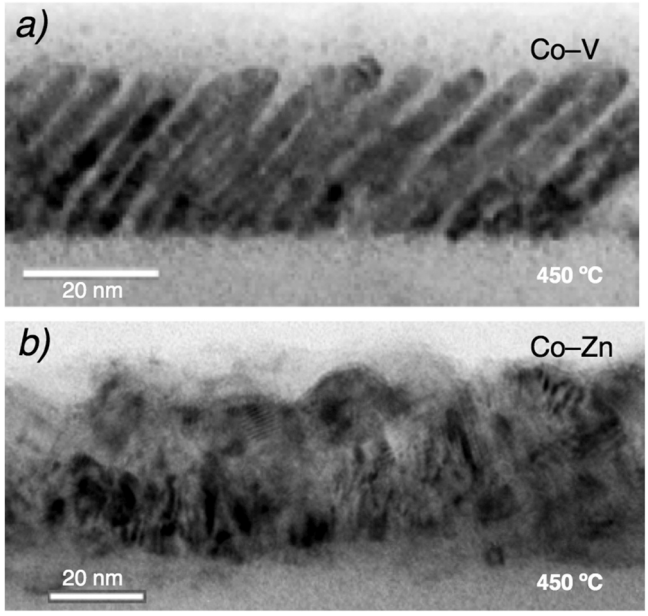

Fig. 5. HRTEM images showing the cross-sections of 450 ºC annealed CSOG films. Two important facts are observed: (a) The Co–V film retains anisotropic nano-sheet morphology, although numerous crystals have grown inside the nano-sheets; (b) the Co–Zn film has lost its nano-sheet morphology, which has been replaced by randomly distributed crystals. The important role of the different spatial distribution of V or Zn in the Co–V and Co–Zn as-deposited CSOG samples is clear. See Fig. 4 and text for an explanation.

which the charges moved along a perpendicular direction ($R_{\perp}$). The mean free path of the electric charges was larger when the conduction occurred inside a nano-sheet than when the conduction was produced by traveling across the nano-sheets, that is, a nano-sheet with insufficient contact with its neighboring nano-sheets (except at the contact points between them). This reasoning is confirmed by the observation of the nano-sheets.

After annealing (Tann. = 450 °C), despite the changes in R, remarkably, these Co–V CSOG films quantitatively retained the proportion of the difference between the new $R_{\perp,ann}$ and $R_{\parallel,ann}$ with respect to the new $R_{\parallel,ann}$ value, as shown by the measurements in Table 1. $R_{\perp}$ and $R_{\parallel}$ were different in the as-deposited state and were different after annealing; the percent of $(R_{\perp}- R_{\parallel})/R_{\parallel}$ was maintained, revealing that the Co–V CSOG films were, from an electrical point of view, approximately equally anisotropic in both states. Based on these measurements, the films' electrical conductivity could be understood as exhibiting two modes: one corresponding to the nano-sheets, reflected in $R_{\parallel}$, and another one associated with the inter-nano-sheet conduction. Notably, the $(R_{\perp} - R_{\parallel})/ R_{\parallel}$ ratio was not affected by the thermal treatment at least up to 450 °C. Also the 33% anisotropy in the resistance of the as-deposited Co–V CSOG films was higher than the ≈ 24% corresponding to the as-deposited anisotropic Co CSOG film [32]. This could have been due to the presence and higher concentration of vanadium atoms in the region between nano-sheets, playing the role of impurities, as can be observed in Fig. 4(a). This would increase the value of $R_{\perp}$ with respect to $R_{\parallel}$, which mostly depended on the inner region of the nano-sheets.

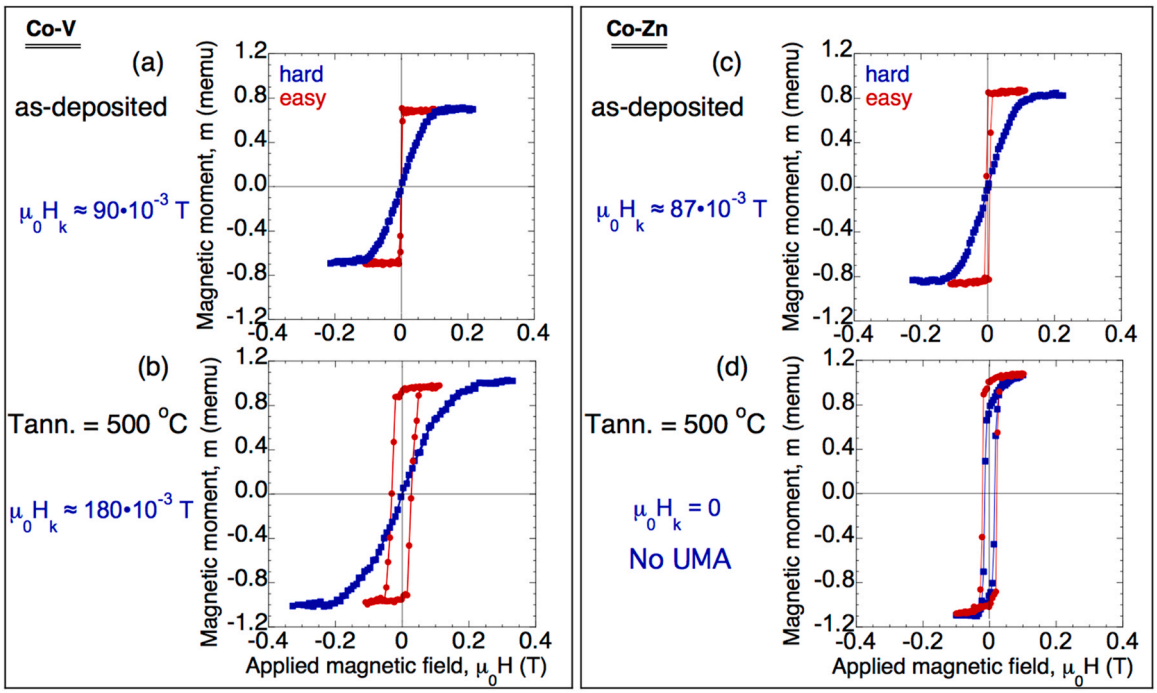

Fig. 6. In-plane *M–H* hysteresis loops corresponding to the (a) as-deposited Co–V CSOG film, (b) Co–V CSOG annealed at 500 °C, (c) as-deposited Co–Zn CSOG film, and (d) Co–Zn CSOG annealed at 500 °C. The hard direction (blue square symbols) and easy direction (red circle symbols) are shown. In the annealed films, the uniaxial magnetic anisotropy increased for the Co–V and this anisotropy was lost for the Co–Zn. The solid lines provide visual guides.

Table 1
Electrical resistance *R* of the Co–V CSOG film and the Co–Zn CSOG film measured at room temperature. *R* was measured (schematically drawn) parallel to the nano-sheets, $R_{||}$, and perpendicular to thse nano-sheets, $R_{\perp}$. For the Co–V films, $R_{\perp}$ and $R_{||}$ were different in the as-deposited state and were different after annealing. The difference $(R_{\perp}- R_{||})/R_{||}$ was maintained. On the contrary, for the Co–Zn, $R_{\perp}$ and $R_{||}$ were different in the as-deposited state, but they were equal after annealing.

Sample	Stage	$R_{||}$ (Ω)	$R_{\perp}$ (Ω)	$[(R_{\perp} - R_{||})/R_{||}]$ (%)
Co–V	*As-deposited*	180 ± 2	239 ± 4	≈ 33
	$T_{ann.}$ = 450 ºC	90 ± 1	118 ± 1	≈ 31
Co–Zn	*As-deposited*	229 ± 3	297 ± 5	≈ 18
	$T_{ann.}$ = 450 ºC	48 ± 1	48 ± 1	0

Co–Zn CSOG films, *R(T = 20 ºC)*: The as-deposited samples were also, like the Co–V CSOG and the pure Co CSOG films [32], electrically anisotropic, with $(\Delta R/R_{||})_{as\text{-}dep.} \approx 18\%$; these facts were in accordance with their magnetic anisotropies and, above all, as a consequence of their nano-sheet morphology. Regarding the lower value of 18% with respect to the 33% of the Co–V CSOG film and the 24% of pure Co CSOG, despite the nano-sheet morphology being common for both, we must consider the presence of Zn nanocrystals (Fig. 1b, and Fig. 4c) which firstly reduced the volume of the nano-sheet region with respect to the total volume of the film, thus reducing the anisotropy behavior, and, secondly, the expected isotropic behavior of these Zn nanocrystals versus the anisotropic one of the nano-sheets. All of this occurred versus the homogeneously extended mixture of Co nanocrystals, 1–2 nm in size, and V nanocrystals or atoms, 1–2 nm in size, in the anisotropic nano-sheets of the Co–V CSOG films (Figs. 1(a) and 4(a)).

The annealed Co–Zn CSOG samples completely lost their electrical transport anisotropy, as shown in Table 1. Both parallel and perpendicular resistances at room temperature were equal after the annealing. This loss had its origin in the disappearance of the nano-sheets (Fig. 4(c) and Fig. 5(b)), which were the source of the transport anisotropy of the as-deposited samples, as we previously demonstrated. There was no discontinuity in the interior of the samples and no free space among the nano-sheets (as they no longer existed), so the mean free path of the electric charges was equal in any direction of measurement. Regarding this behavior, it is important to note its similarity to the results exhibited by the CSOG films of pure Co initially formed by oblique nano-sheets, which lost the anisotropy [31,32], contrary to the Co–V CSOG films.

3.3.2. Resistance variation with temperature

To obtain further insight into the anisotropic behavior observed for the transport properties of these CSOG films, the dependence of the resistance *R* on temperature was measured. This is a structure-sensitive property that is directly related to the atomic diffusion processes induced in the material and, consequently, is linked to the nano-morphology [32]. Fig. 7 shows the results of *R* vs. *T* for these Co–V and Co–Zn CSOG films. The measurements were recorded in the $R_{||}$ as well as in the $R_{\perp}$ configurations. The first result obtained from these measurements was the visualization of the irreversible processes activated for both types of CSOG film, Co–V and Co–Zn, in the interval of temperatures from 20 to 450 ºC, as is expected for nano-crystalline or amorphous materials out of thermodynamic equilibrium (at 20 ºC).

Co–V CSOG films, *R(T)*: The values and the evolution of $R_{||}(T)$ and $R_{\perp}(T)$ were different in all of the states as shown in Fig. 7(a): At room temperature in the as-deposited state, during the annealing, and at room temperature after the heating. $R_{\perp}$ was always higher than $R_{||}$ during the whole interval; the anisotropic property was preserved for this temperature interval. This reinforced the reasoning that the films' electrical conductivity along the nano-sheets was different from the conductivity transverse to those.

As the perpendicular resistance $R_{\perp}$ displayed its first significant change between 70 and 290 ºC, Fig. 7(a), the first structural relaxation processes must have occurred. Since, for this interval, the parallel resistance $R_{||}$ remained constant, the corresponding relaxation processes did not affect the parallel conduction (they did not affect the intra-longitudinal nano-sheet conduction); that is, the first

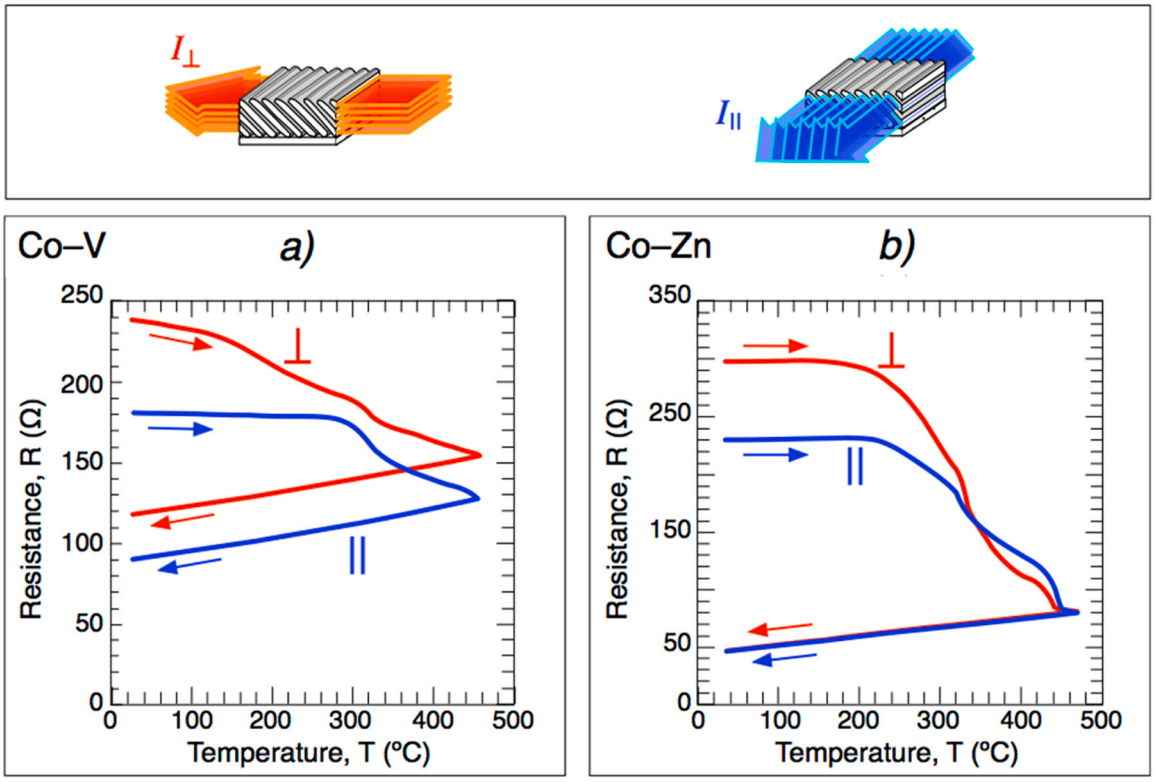

Fig. 7. Dependence of the resistance *R* on the temperature for the oriented nano-sheet-formed (a) Co–V CSOG films and (b) Co–Zn CSOG films. The arrows indicate the variation in temperature, increasing or decreasing, for each continuous process of measurement of *R*(T). The red curves indicate the measurements perpendicular to the nano-sheets and the blue curves are the measurements parallel to the nano-sheets. The upper section of the figure shows two diagrams of the direction of the current, $I_{||}$ and $I_\perp$, with respect to the direction of the nano-sheets.

relaxation processes occurred at the interconnection points between nano-sheets (probably the more unstable atoms, that is, atoms more weakly bonded) and at the inter-nano-sheet region rich in V, see Fig. 4(a) and Fig. 5(a). From 290–450 ºC, the corresponding structural relaxation processes had similar consequences for both measured resistances $R_{||}$ and $R_\perp$, and consequently, these relaxation processes must have been produced in the inner region of nano-sheets, since both resistances corresponded to conduction through the nano-sheets, longitudinally for $R_{||}$ and transversely for $R_\perp$. These *R* vs. *T* measurements allowed us to discriminate between the atomic phenomena of relaxation that happened in the region between the nano-sheets with respect to those in the core of these nano-sheets. The relaxation processes at temperatures above 290 ºC, which affected the inner part of nano-sheets, and therefore both $R_{||}$ and $R_\perp$ resistances, had different consequences in terms of the parallel resistance, $\Delta R_{||}$, and the perpendicular resistance, $\Delta R_{||\,(290\ ºC->450ºC)} \approx 2\,\Delta R_{\perp(290\ ºC->450ºC)}$. This behavior finally produced a total retention with a 33% difference between both resistances or total retention of the anisotropic transport property of the Co–V CSOG films with oblique nano-sheets.

Comparing this behavior with that of the PLD Co CSOG films with oblique nano-sheets [32], we observed two large and essential differences between them. Firstly, for the Co film and for temperatures above 290 ºC—temperatures at which the first relaxation processes of the perpendicular resistance $R_\perp$ had been completed—both $R_{||}$ and $R_\perp$ continued their relaxation processes together with the same shape and values; that is, the Co CSOG film was electrically isotropic above 290 ºC. In contrast, the Co–V CSOG film never had the same values for $R_\perp$ and $R_{||}$ for temperatures between 20 and 450 ºC; that is, it was, and remained, electrically anisotropic in that interval. Secondly, for the Co CSOG film, the decrease in the resistance after the total structural relaxation was more than 90%, whereas the Co–V CSOG film displayed a decrease in its resistance of approximately 50%; that is, the Co–V film underwent total structural relaxation processes that were very weak compared with the Co film. The Co–V CSOG film was much more stable than the Co CSOG film, at least up to 500 ºC.

Co–Zn CSOG films, *R(T)*: Both curves $R_{||}(T)$ and $R_\perp(T)$ remained constant up to temperatures of 160–170 °C, (Fig. 7(b)). Therefore, no indications of structural relaxation or modifications were visible from room temperature to 160–170 °C in any of the curves; the structure of the Co amorphous nano-sheets with the Zn nanocrystals, see Fig. 4(c), was thermally stable up to this temperature. The anisotropic resistance of these films was retained up to 160–170 ºC, when the first relaxation processes started and both $R_{||}$ and $R_\perp$ started to change, with the same value also being achieved for approximately 330 ºC. A larger decrease in the perpendicular resistance $R_\perp$ than that corresponding to $R_{||}$, suggested that the relaxation processes that occurred between 160 and 170 and 330 ºC mostly affected the region between nano-sheets, resulting in the disappearance of the initial morphology of nano-sheets. From this temperature until 470 ºC (the maximum annealing temperature achieved in these *R*(*T*) measurements), $R_{||}$ and $R_\perp$ mostly maintained the same value; that is, the anisotropic resistance of these films was lost at 330 ºC and they evolved to isotropic films because both exhibited the same value at room temperature after the annealing processes up to 470 ºC. Therefore, between 330 and 470 ºC, once the nano-sheets disappeared, the anisotropic property consequently disappeared, and the corresponding relaxation processes similarly affected the parallel and perpendicular resistances.

Comparing this behavior with that of the PLD Co CSOG films with oblique nano-sheets [32], we observed two large and essential similarities between them. Firstly, for the Co film, the decrease in $R_\perp$ from 140 to 290 ºC was larger than that corresponding to $R_{||}$, having

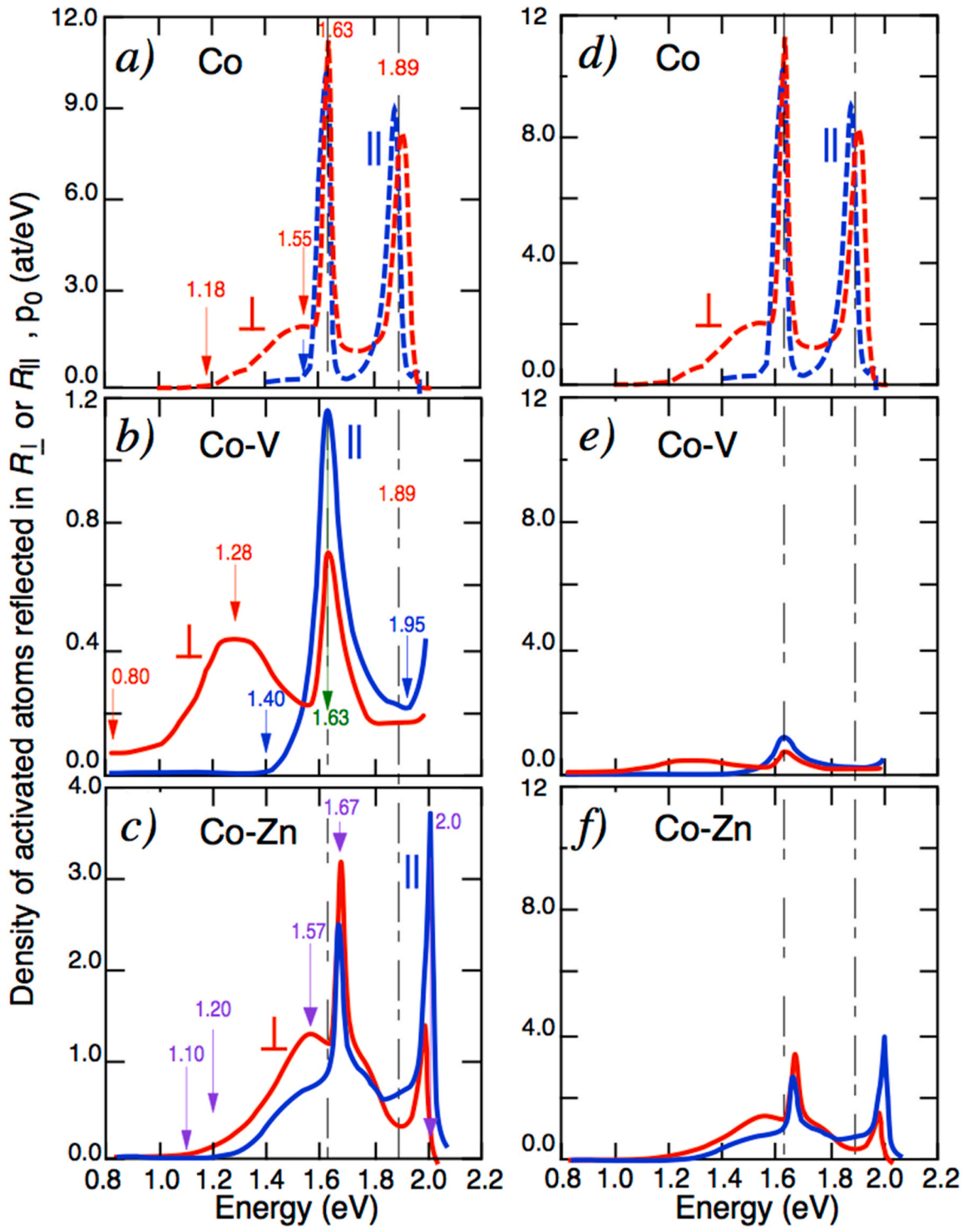

Fig. 8. Activation energy spectra of the processes that occurred during annealing of the CSOG films, which affected the resistance, obtained from the measurements of the resistance dependence on temperature: (a) Co [32], (b) Co–V, and (c) Co–Zn CSOG films, for R_{II} (T) and $R_{\perp}$(T). The vertical arrows indicate the values of the activation energy for the beginning of changes, the maxima, or the peaks of activated atomic processes. (d, e, and f) The same three films with the same vertical scales for comparison of the intensity of the relaxation phenomena.

the same value at 290 ºC. The Co–Zn CSOG film displayed similar behavior between 160 and 170 and 330 ºC; that is, the Co–Zn film lost its anisotropic resistance behavior at 330 ºC and the Co film also lost its anisotropic resistance at 290 ºC. Secondly, for the Co film and for temperatures above 290 ºC, at which point the first relaxation processes of $R_{\perp}$ were completed, both R_{II} and $R_{\perp}$ continued their relaxation processes together with the same shape and values; the Co CSOG film was electrically isotropic above 290 ºC. Similarly, the Co–Zn CSOG film had approximately the same values for $R_{\perp}$ and R_{II} for temperatures between 330 and 450 ºC; that is, it was, and remained, electrically isotropic in this interval. Both films with an initial oblique nano-sheet morphology had similar behavior, losing their transport anisotropy for low temperatures, 290 ºC for the Co films and 330 ºC for the Co–Zn films.

Table 2
Activation energies E_0 of structural relaxation processes linked to the perpendicular resistance $R_\perp$ or parallel resistance $R_{||}$, corresponding to different Co [32], Co–Zn, and Co–V anisotropic CSOG films formed by oblique nano-sheets. $T_{m.heat.}$ is the measured temperature during heating corresponding to E_0. The superscripts indicate similar relaxation processes corresponding to equal or very close energies and different materials. The crystalline (or not) structure of the films is also shown where "–Zn" means except Zn nanocrystals. The morphology of the films formed by nano-sheets (or not) is also indicated. The last column corresponds to the presence (or not) of uniaxial magnetic anisotropy in the film; its persistence in the sample of Co–V for the highest energy can be noted.

E_0 (eV)	$T_{m.heat.}$ (ºC)	Activated relaxation processes		Crystalline X-ray peaks	NANO-SHEET MORPHOLOGY	UNIAXIAL ANISOTROPY
		Stage	Affected magnitude			
0.80	22	Beginning	R ⊥ of Co–V	No	Yes	Yes
1.10 *	127	Beginning	R ⊥of Co–Zn	No(–Zn)	Yes	Yes
1.18 *	156	Beginning	R ⊥of Co	No	Yes	Yes
1.20	163	Beginning	$R_{||}$ of Co–Zn	No(–Zn)	Yes	Yes
1.28	191	MAXIMUN	R ⊥ of Co–V	No	Yes	Yes
1.40	233	Beginning	$R_{||}$ of Co–V	No	Yes	Yes
1.55	286	Beginning	$R_{||}$ – Co	No	No	No
1.55 **	286	MAXIMUN	R ⊥ – Co	No	No	No
1.57 **	293	MAXIMUN	R ⊥– Co–Zn	No(–Zn)	No	No
1.63[x]	314	PEAK-1	$R_{||}$ and R ⊥ – Co	No	No	No
1.63[x]	314	PEAK-1	$R_{||}$ and R ⊥of Co–V	No	Yes	Yes
1.67[x]	328	PEAK-1	$R_{||}$ and R ⊥of Co–Zn	No(–Zn)	No	No
1.89	405	PEAK-2	$R_{||}$ and R ⊥of Co	Yes	No	No
1.95	425	Beginning-2	$R_{||}$ and R ⊥of Co–V	Yes	Yes	Yes
2.00	443	PEAK-2	$R_{||}$ and R ⊥of Co–Zn	Yes	No	No
2.02	450	Increasing	$R_{||}$ of Co–V	Yes	Yes	Yes

3.3.3. Analysis of the energy of structural relaxation processes

To analyze and compare the different structural relaxation processes activated by high temperatures in Co [32], Co–V, and Co–Zn CSOG films comprising oblique nano-sheets, we studied the evolution of their corresponding resistances with respect to the energy required to cause relaxation processes.

The activation energy spectra of the atomic processes that occurred during annealing of the Co–V and Co–Zn were obtained within the framework of Primark's model [42,43] as previously reported for pure Co films [32]. The annealing temperature T was related to the activation energy E_0 by the equation $E_0 = (kT/b)$ [ln $(\upsilon_0 T/V_s)$ -a], where k is the Boltzmann constant, υ_0 is the Debye frequency for single atom jumps (we assumed 10^{12} s^{-1}, as in [32,42]), V_s is the annealing rate (0.17 K s^{-1} in our experiments), and a and b are fitted parameters considering the approximations detailed in [42,43] (mainly that E_0/kT + ln[(E_0/kT)+ 2] ≈ a + $(E_0/kT)b$)). For the determination of parameters a and b using this approximation, we used the interval 0.5–2.5 eV, typical for structural relaxation phenomena in amorphous materials [43,44]. We obtained a = 2.6 and b = 1.03 for the best fit, as was used in Ref. 32. Therefore, the activation energy spectrum p_0 was calculated using variation of the resistance R with temperature and the equation $p_0 = (-1/R_0)(dR/dT)(dE_0/dT)^{-1}$, where R_0 is the value of the resistance in the as-deposited state [42].

Fig. 8 shows the calculations for both $R_{||}$ and $R_\perp$ for the Co [32], Co–V, and Co–Zn CSOG films.

In Fig. 8(a, b, c), we indicate, with vertical arrows, the values of the energy that activated the relaxation of atoms, which affected the values of the perpendicular resistance, the parallel resistance, or both resistances. We considered the evolution of the resistances, in particular, the beginning of changes, maximal values, and peaks in this evolution. The changes produced in the properties of the films by these annealing processes were always irreversible. Interesting results were obtained after these studies: Similar or close measurements for the Co and Co–Zn CSOG films or, conversely, important differences for the Co–V CSOG samples with respect to the Co and Co–Zn CSOG films, although the three materials presented the common Co-rich characteristic and the common nano-sheet morphology. Table 2 shows a set of these singular points in terms of the energy values.

For a low energy, from 0.80 eV, the relaxation processes started and affected the perpendicular resistance $R_\perp$ of the Co–V CSOG film, reaching the maximum at 1.28 eV. For this broad interval of energy, the corresponding relaxation processes did not affect the parallel resistance $R_{||}$. Only the very weakly bonded atoms, located at the contact points between nano-sheets or at the surface of the nano-sheets, including inter-nano-sheet regions, relaxed. This relaxation of atoms, probably V or Co surrounded by V, did not break the morphology of the film comprising nano-sheets (Fig. 4(a)), maintaining the uniaxial magnetic anisotropy, (Fig. 6(b)), and the transport anisotropy, $R_\perp$ different from $R_{||}$ (Fig. 7(a)). The presence of V atoms avoided the coalescence of nano-sheets, due to the location of these atoms being predominantly at the inter-nano-sheets, and also due to their low mobility at these relatively low temperatures (the melting temperature for V is 1890 ºC). This spatial distribution of atoms allowed the presence of uniaxial magnetic anisotropy due to the small Co nanocrystals that were predominantly located at the core of the preserved nano-sheets, see Fig. 5(a). As such, the sources of the magnetic properties of the Co–V CSOG films retained the necessary magnetic nano-sheet image, which produced their uniaxial magnetic anisotropy. The vanadium atoms protected this nano-morphology of the Co–V CSOG films.

At 1.10 and 1.18 eV, the relaxation processes of Co and Co–Zn CSOG films began, respectively. This relaxation also affected their perpendicular resistance $R_\perp$, and was extended for both films until the energies of 1.55 and 1.57 eV, when the maxima in the corresponding spectra were achieved. As was demonstrated in Ref. 32 for Co CSOG, for these energy values, the film's nano-sheet morphology was destroyed and the films lost their uniaxial anisotropy. The location of Zn (Fig. 4(c)) favored the rest of the volume of the Co–Zn film, mostly Co, exhibiting a behavior similar to the pure Co film. With these relaxation processes, the Co–Zn film lost its anisotropic property, similar to the Co films. From this activation energy value, corresponding to ≈ 286 and 293 ºC, $R_\perp$ started its approximation to $R_{||}$ (Fig. 7(b)). Although this relaxation process also affected its $R_{||}$, probably due to the relaxation of the nano-crystals of zinc (Fig. 8(c)), this did not avoid approximation between the $R_\perp$ and $R_{||}$ values (Fig. 7(b)); that is, it did not avoid the loss of uniaxial anisotropy.

For energies above 1.40–1.55 eV, the relaxation processes started affecting $R_{||}$ in the Co–V and Co CSOG films; that is, the relaxation processes also started to be located in the core of the nano-sheets of Co–V CSOG films, but this was different to the cases of Co and Co–Zn CSOG, as these had lost their nano-sheet morphology and evolved to form a mostly isotropic state. The continuous approximation between the values of $R_\perp$ and $R_{||}$ for Co [32] and Co–Zn films (Fig. 7(b)), with similar peaks at 1.63 and 1.67 eV, ≈ 314–328 ºC, corresponded to Co relaxation in the amorphous state, or to the atoms on the frontier

of nanocrystals and no growth, as shown in the X-ray diffractogram [32].

The large peak in the relaxation of $R_{\perp}$ and $R_{||}$ between 1.42 and 1.85 eV, centered at 1.63 eV for the Co–V CSOG film, affected both the inter-nano-sheet regions and the frontiers of the nano-sheets and their inner region, and corresponded to the nano-crystalline state of Co and of Co–V. The nano-sheet morphology and, consequently, the uniaxial anisotropy were preserved by this relaxation phenomenon.

At 1.89 eV [32], the Co CSOG films exhibited the second peak of relaxation of $R_{\perp}$ and $R_{||}$ produced by the isotropic crystallization of *hcp* Co.

At 1.96 eV, the Co–V CSOG films started the second relaxation process, which affected $R_{||}$ and weakly $R_{\perp}$, indicating that the relaxation phenomenon was principally located in the inner region of the nano-sheets. This process was the origin of the crystallization of the Co and Co–V amorphous phases, which were still constituents of the nano-sheets of the film. Thus, the new crystals of *hcp* Co and Co_3V generated the corresponding crystalline peaks in the X-ray diffractogram (Fig. 1(a)). This last crystallization reinforced the morphology of these Co–V films formed by nano-sheets and the uniaxial magnetic anisotropy of these films.

For 2.0 eV, the Co–Zn CSOG films showed the second peak of relaxation for both $R_{\perp}$ and $R_{||}$, which was due to the ending of the growth of the *hcp* Co and to the crystallization of β–CoZn and γ–CoZn phases, in accordance with Fig. 1(b) and Fig. 5(c), remaining as the isotropic conductor.

Regarding the quantitative behavior of these relaxation phenomena, we present the energy spectra in Fig. 8(d, e, f) using the same scale for the three materials: Co, Co–V, and Co–Z. In particular, and considering $R_{\perp}$ whose relaxation processes were accompanied by the loss of the nano-sheet morphology for Co and Co–Zn CSOG films, the fraction of relaxed atoms in an interval of energy with limits $E_{0,1}$ and $E_{0,2}$, with $R_{\perp,1}$ and $R_{\perp,2}$ being the corresponding values of the affected magnitude by relaxation, (represented by the integral of the parameter p_0dE extended to that interval), was $\Delta R_{\perp \text{interval}} / R_{\perp 0}$, where $\Delta R_{\perp \text{interval}} = R_{\perp,2} - R_{\perp,1}$ and $R_{\perp 0} = R_{\perp}$(20 ºC, before relaxation). The value from cobalt´s CSOG spectrum (Fig. 8(d)) had the relation of 0.31:0.30 = 1.03 times and 0.31:0.20 = 1.55 times with respect to the corresponding fraction of relaxed atoms in the Co–Zn CSOG films and Co–V CSOG films, respectively (in accordance with the different increases in the resistance shown in Fig. 7). The presence of the zinc atoms weakly reduced the mobility of Co atoms for the inter-nano-sheet relaxation to 97%, not enough to slow the destruction of the nano-sheets. Differently, the presence of vanadium atoms strongly reduced the mobility of atoms to 65%, so the nano-sheets were then capable of enduring, avoiding their coalescence and consequent destruction. Moreover, the subsequent crystallization processes reinforced the firmness of the Co–V nano-sheets; consequently, the uniaxial magnetic anisotropy was increased.

In summary, both Co and Co–Zn CSOG films lost their anisotropy at 1.57 eV (293 ºC) when they lost their nano-sheet morphology, evolving into in-plane isotropic films. Their structure remained non-crystalline, except for the Zn nanocrystals, and the subsequent crystallization processes retained and reinforced this isotropic property.

The Co–V CSOG films retained their nano-sheet morphology from the initial non-crystalline structure to the final mainly crystalline structure, remaining anisotropic until at least an energy of 2.02 eV at 450 ºC, when the uniaxial magnetic anisotropy was reinforced. Even after annealing at 500 ºC, this UMA was preserved. The structural relaxation processes did not break this nano-sheet morphology. The growth of *hcp* Co and Co_3V in their preserved nano-sheets caused the uniaxial magnetic anisotropy of these Co–V CSOG films to be not only preserved, but also enhanced.

4. Conclusions

The anisotropic magnetic and transport properties of Co–V and Co–Zn Cylindrical Symmetry Oblique Growth (CSOG) thin films were studied. The main and new findings of this work are listed below:

Co–V and Co–Zn CSOG thin films showed a morphology of oblique nano-sheets. These nano-sheets were formed by amorphous rich in Co: Co ≈ 80%–V ≈ 20% for Co–V films and Co ≈ 98%–Zn ≈ 2% for Co–Zn films. The inter-nano-sheet spaces were occupied by: (a) an abundance of atoms of V or amorphous V, ≈ 60% Co relative to ≈ 40% V in Co–V CSOG films; or (b) very few atoms of Zn, ≈ 93% Co relative to ≈ 7% Zn in the Co–Zn films, with Zn segregated at the bottom of the film. After annealing the films at 450 ºC, the Co–V films retained their oblique nano-sheets, which comprised *hcp* Co and Co_3V. In contrast, the Co–Zn films lost their nano-sheet morphology evolving to an isotropic distribution of *hcp* Co and β–CoZn and γ–CoZn.

The effect of heating processes can be described by three stages:

(1) Structural relaxation phenomena at low activation energies from 0.80 to 1.57 eV at inter-nano-sheet regions. Only atoms located at the contact points between nano-sheets or at the inter-nano-sheets regions were activated. For Co–V films, at the energy of 1.28 eV, the nano-sheet morphology was preserved and, consequently, their uniaxial anisotropy was also preserved. The Co and Co–Zn films displayed coalescence of the nano-sheets at 1.55–1.57 eV; consequently, they lost the uniaxial anisotropy property.
(2) Structural relaxation processes at medium activation energies from 1.57 to 1.80 eV in the inner region of the nano-sheets. At 1.63 and 1.67 eV, the Co and Co–Zn films, retained their non-crystalline nature (except the Zn crystals), as the Co–V films.
(3) Crystallization processes at high activation energies from 1.80 to 2.2 eV in the inner of nano-sheets in Co–V film and in the whole Co–Zn film. For Co and Co–Zn films the crystallization of Co and β–CoZn and γ–CoZn at the peak of 1.89 and 2.0 eV reinforced the isotropic behavior of these films. For Co–V anisotropic films, at 1.95 eV, the crystallization of *hcp* Co and Co_3V in the intra-nano-sheet regions started, which increased the uniaxial anisotropy property of the films, which were maintained at least up to 2.2 eV.

These anisotropic Co–V and Co–Zn CSOG films can be useful in spintronic sensor technology, magneto-electrical, magneto-mechanical devices… emphasizing the preservation at high temperatures of the anisotropic nature of Co–V compounds, since they could be used for these applications at high temperatures by preserving their anisotropic behavior.

CRediT authorship contribution statement

C. Favieres: Conceptualization, Methodology, Formal analysis, Investigation, Writing - original draft, Writing - review & editing, Visualization. **J. Vergara:** Formal analysis, Investigation, Writing - review & editing, **C. Magén:** Investigation, Writing - review & editing, **M.R. Ibarra:** Investigation, Writing - review & editing, **V. Madurga:** Conceptualization, Methodology, Formal analysis, Investigation, Writing - review & editing, Visualization.

Declaration of Competing Interest

The authors declare that they have no known competing financial interests or personal relationships that could have appeared to influence the work reported in this paper.

Acknowledgments

C. F., J. V., and V. M. acknowledge the financial support of the Public University of Navarre. C.M. and M.R.I. acknowledge the financial support from the Spanish Ministerio de Economía y Competitividad in the project MAT2017–82970-C1 and C2-R and from the Aragón Regional project E26. Open access funding provided by Universidad Pública de Navarra.

References

[1] R.P. Cowburn, Property variation with shape in magnetic nanoelements, J. Phys. D: Appl. Phys. 33 (2000) R1–R16.
[2] T. Shinjo, Nanomagnetism and Spintronics, second ed., Elsevier, Amsterdam, 2014.
[3] J.F. Bobo, L. Gabillet, M. Bibes, Recent advances in nanomagnetism and spin electronics, J. Phys.: Condens. Matter 16 (2004) S471–S496, https://doi.org/10.1088/0953-8984/16/5/008
[4] C. Chappert, A. Barthelémy, Nanomagnetism and spin electronics, in: C. Dupas, P. Houdy, M. Lahnmany (Eds.), Nanoscience, Springer, Berlin, 2007, pp. 503–582.
[5] June W. Lau, Justin M. Shaw, Magnetic nanostructures for advanced technologies: fabrication, metrology and challenges, J. Phys. D: Appl. Phys. 44 (303001) (2011) 41, https://doi.org/10.1088/0022-3727/44/30/303001
[6] J.P. Liu, E. Fullerton, O. Gutfleisch, D.J. Sellmyer, Nanoscale Magnetic Materials and Applications (Eds.), Springer, New York, 2006.
[7] Atsufumi Hirohata, Keisuke Yamada, Yoshinobu Nakatani, Ioan-Lucian Prejbeanu, Bernard Diény, Philipp Pirro, Burkard Hillebrands, Review on spintronics: Principles and device applications, J. Magn. Magn. Mater. 509 (166711) (2020) 28, https://doi.org/10.1016/j.jmmm.2020.166711
[8] Cheng Gong, Xiang Zhang, Two-dimensional magnetic crystals and emergent heterostructure devices, Science 363 (706) (2019) 706.10.1126/science. aav4450.
[9] Sabpreet Bhatti, Rachid Sbiaa, Atsufumi Hirohata, Hideo Ohno, Shunsuke Fukami, S.N. Piramanayagam, Spintronics based random access memory, Mater. Today 20 (2017) 530–548, https://doi.org/10.1016/j.mattod.2017.07.007
[10] E.Y. Vedmedenko, R.K. Kawakami, D.D. Sheka, P. Gambardella, A. Kirilyuk, A. Hirohata, C. Binek, O. Chubykalo-Fesenko, S. Sanvito, B.J. Kirby, J. Grollier, K. Everschor-Sitte, T. Kampfrath, C.-Y. You, A. Berger, The 2020 magnetism roadmap (44pp), J. Phys. D: Appl. Phys. 53 (2020) 453001, https://doi.org/10.1088/1361-6463/ab9d98
[11] Stuart Parkin, Xin Jiang, Christian Kaiser, Alex Panchula, Kevin Roche, Mahesh Samant, Magnetically engineered spintronic sensors and memory, IEEE 91 (2003) 661–680, https://doi.org/10.1109/JPROC.2003.811807
[12] J.M. De Teresa, A. Fernández-Pacheco, R. Córdoba, L. Serrano-Ramón, S. Sangiao, M.R. Ibarra, Review of magnetic nanostructures grown by Focused Electron Beam Induced Deposition (FEBID) (24 pp), J. Phys. D: Appl. Phys. 49 (2016) 243003, https://doi.org/10.1088/0022-3727/49/24/243003
[13] P.N. Solovev, A.V. Izotov, B.A. Belyaev, Microstructural and magnetic properties of thin obliquely deposited films: a simulation approach, J. Magn. Magn. Mater. 429 (2017) 45–51, https://doi.org/10.1016/j.jmmm.2017.01.012
[14] Amalio Fernández-Pacheco, Robert Streubel, Olivier Fruchart, Riccardo Hertel, Peter Fischer, Russell P. Cowburn, Three-dimensional nanomagnetism (814 pp), Nat. Commun. 8 (2017) 15756, https://doi.org/10.1038/ncomms15756
[15] K. Watanabe, B. Jinnai, S. Fukami, H. Satom, H. Ohno, Shape anisotropy revisited in single-digit nanometer magnetic tunnel junctions, Nat. Commun. 9 (663) (2018) 6, https://doi.org/10.1038/s41467-018-03003-7
[16] O. Tosun, I. Ruzybayev, F.M. Abel, B. Balamurugan, R. Skomski, D.J. Sellmyer, G.C. Hadjipanayis, Structural and magnetic properties of Co–V nanoparticles (5 pp), AIP Adv. 9 (2019) 125144, https://doi.org/10.1063/1.5130456
[17] Cuiping Wang, Cancan Zhao, Yong Lu, Tian Li, Dongliang Peng, Ji Shi, Xingjun Liu, Experimental observation of magnetically induced phase separation and thermodynamic assessment in the Co–V binary system, Mater. Chem. Phys. 162 (2015) 555–560, https://doi.org/10.1016/j.matchemphys.2015.06.028
[18] Sean W. Fackler, Vasileios Alexandrakis, Dennis König, A.Gilad Kusne, Tieren Gao, Matthew J. Kramer, Drew Stasak, Kenny Lopez, Brad Zayac, Apurva Mehta, Alfred Ludwig, Ichiro Takeuchi, Combinatorial study of Fe-Co–V hard magnetic thin films, Sci. Technol. Adv. Mater. 1 (2017) 231–238, https://doi.org/10.1080/14686996.2017.1287520
[19] A. Manouchehri, A. Ramazani, M. Almasi Kashi, A.H. Montazer, Tunable magnetocrystalline easy axis in cobalt nanowire arrays by zinc additive, Mater. Sci. Eng. B 207 (2016) 18–25, https://doi.org/10.1016/j.mseb.2016.01.008 0921-5107
[20] Chengyi Hou, Hao Yu, Qinghong Zhang, Yaogang Li, Hongzhi Wang, Preparation and magnetic property analysis of monodisperse Co–Zn ferrite nanospheres, J. Alloy. Compd. 491 (2010) 431–435, https://doi.org/10.1016/j.jallcom.2009.10.217
[21] T.G. Knorr, R.W. Hoffman, Dependence of geometric magnetic anisotropy in thin Iron films, Phys. Rev. 113 (1959) 1039–1046.
[22] Yao Zhang, Qingfeng Zhan, Zhenghu Zuo, Huali Yang, Xiaoshan Zhang, Guohong Dai, Yiwei Liu, Ying Yu, Jun Wang, Baomin Wang, Run-Wei Li, Magnetization reversal in epitaxial exchange-biased IrMn/FeGa bilayers with anisotropy geometries controlled by oblique deposition, Phys. Rev. B 91 (2015) 174411, https://doi.org/10.1103/PhysRevB.91.174411
[23] Y.-P. Zhao, D.-X. Yeb, G.-C. Wangb, T.-M. Lub, Designing nanostructures by glancing angle deposition, in: A. Lakhtakia, S. Maksimenko (Eds.), Proceedings of SPIE Vol. 5219 Nanotubes and Nanowires, SPIE, Bellingham, WA, 2003, pp. 59–73.
[24] V. Madurga, J. Vergara, C. Favieres, Magnetic domain structures and nano-string morphology of laser off-normal deposited amorphous cobalt films with controlled magnetic anisotropy, J. Magn. Magn. Mater. 272–276 (2004) 1681–1683, https://doi.org/10.1016/j.jmmm.2003.12.251
[25] J. Shena, Zheng Gaib, J. Kirschner, Growth and magnetism of metallic thin films and multilayers by pulsed-laser deposition, Surf. Sci. Rep. 52 (2004) 163–218, https://doi.org/10.1016/j.surfrep.2003.10.001
[26] Lulu Pan, Fenglong Wang, Wenfeng Wang, Guozhi Chai, Desheng Xue, In-plane isotropic microwave performance of CoZr trilayer in GHz range (7 pp). Sci. Rep. 6 (2016) 21327, https://doi.org/10.1038/srep21327
[27] Nguyen N. Phuoc, Feng Xu, C.K. Ong, Tuning magnetization dynamic properties of Fe–SiO2 multilayers by oblique deposition (4 pp). J. Appl. Phys. 105 (2009) 113926, https://doi.org/10.1063/1.3143042
[28] Johanna K. Jochuma, Thomas Saerbeck, Vera Lazenka, Vincent Joly, Lianchen Shand, Hans-Gerd Boyend, Kristiaan Temst, André Vantomme, Margriet J. Van Bael, Magnetic characterization of oblique angle deposited Co/CoO on gold nanoparticles, J. Magn. Magn. Mater. 483 (2019) 76–82, https://doi.org/10.1016/j.jmmm.2019.03.098
[29] Luran Zhang, Dandan Gao, Huan Liu, Jiyang Xie, Wanbiao Hu, Marked enhancement of roll-off frequency in FeCoN synthetic antiferromagnetic films deposited by oblique incidence (7 pp), Materials 12 (2019) 2328, https://doi.org/10.3390/ma12142328
[30] V. Madurga, C. Favieres, J. Vergara, Growth and sculpting of Co nano-strings on Si micro-cantilevers: magneto-mechanical properties, Nanotechnology 21 (2010) 095702(6 pp) stacks.iop.org/Nano/21/095702.
[31] C. Favieres, J. Vergara, C. Magén, M.R. Ibarra, V. Madurga, Building oriented nano-sheets in thin films of Co-MT (MT = V, Cr, Cu, Zn, Cd, Hf) and the generation and enhancement of their magnetic anisotropy, J. Alloy. Compd. 664 (2016) 695–706, https://doi.org/10.1016/j.jallcom.2015.12.249
[32] J. Vergara, C. Favieres, C. Magén, J.M. De Teresa, M.R. Ibarra, V. Madurga, Structurally oriented nano-sheets in Co thin films: changing their anisotropic physical properties by thermally-induced relaxation (15 pp), Materials 10 (2017) 1390, https://doi.org/10.3390/ma10121390
[33] C. Favieres, J. Vergara, V. Madurga, Tailoring the anisotropic physical properties of thin films for sensors applications by controlling their oblique nano-sheet morphology, J. Mater. Sci. Nanomater. 2 (2018) 2.
[34] B. Chitsazan, H. Shokrollahi, A. Behvandi, O. Mirzaee, Characterization and magnetic coercivity of nanostructured (Fe50Co50)100-xVx= 0,2,4 powders containing a small amount of Co3V intermetallic obtained by mechanical alloying, Powder Technol. 214 (2011) 105–110, https://doi.org/10.1016/j.powtec.2011.07.042
[35] L.J. Nagel, B. Fultz, Phase equilibria of Co_3V, J. Phase Equilibria 100 (1997) 21–23.
[36] B.D. Cullity, S.R. Stock, Elements of X-ray diffraction, Pearson Education International, third ed., Prentice Hall, Inc., New Jersey, 2001, p. 170.
[37] M. Zhao, Z. Wang, F. Yin, Z. Li, Z. Long, Phase equilibria of the Co–Ni–Zn system at 450 °C and 600 °C, Termochim. Acta 545 (2012) 103–111, https://doi.org/10.1016/j.tca.2012.07.002
[38] Hiroaki Nakano, Shitoku Shibata, Shingo Arakawa, Satoshi Oue, Shigeo Kobayashi, Electrodeposition behavior of Zn–Co alloys from an alkaline zincate solution containing triethanolamine, ISIJ Int. 53 (2013) 1858–1863, https://doi.org/10.2355/isijinternational.53.1858
[39] B.D. Cullity, C.D. Graham, Introduction to Magnetic Materials, Second ed., John Wiley & Sons. Inc., Publications, Piscataway, NJ, 2009, p. 320.
[40] Sabrina Lamrani, Abderrahim Guittoum, Rudolf Schäfer, Stefan Pofahl, Volker Neu, Messaoud Hemmous, Nassima Benbrahim, Microstructure investigation and magnetic study of permalloy thin films grown by thermal evaporation (6 pp). Eur. Phys. J. Appl. Phys. 74 (2016) 30302, https://doi.org/10.1051/epjap/2016150548
[41] R.M. Bozorth, Ferromagnetism, D. Van Nostrand Company, Inc, Princeton, New Jersey, 1951, p. 33.
[42] W. Primark, Kinetics of processes distributed in activation energy, Phys. Rev. 100 (1955) 1677–1689.
[43] M. Baricco, P. Allia, F. Vinai, G. Riontino, Structural relaxation in FeNiCrPB amorphous alloys by joint isothermal and tempering measurements of electrical resistivity, J. Mat. Sci. 23 (1988) 4287–4294.
[44] A. Hernando, O.V. Nielsen, V. Madurga, Relaxation processes and pure shear stress creep in a metallic glass ribbon of composition $(Fe_{0.05}Co_{0.95})Si_{15}B_{10}$, J. Mat. Sci. 20 (1985) 2093–2102.